Updating a finite element model to the real experimental setup by thermographic measurements and adaptive regression optimization

Updating a finite element model to the real experimental setup by thermographic measurements and adaptive regression optimization.

J. Peeters[a,*], G. Arroud[a,b], B. Ribbens[a,b,c], J.J.J. Dirckx[c], G. Steenackers[a,b]

[a] *University of Antwerp, Op3Mech, Salesianenlaan 90, B-2660 Antwerp, Belgium. Tel.: +32-3-2051938*
[b] *Vrije Universiteit Brussel, Acoustics & Vibration Research Group, Pleinlaan 2, B-1050, Brussels, Belgium.*
[c] *University of Antwerp, Laboratory of Biomedical Physics, Groenenborgerlaan 171, B-2020 Antwerp, Belgium.*

Abstract

In non-destructive evaluation the use of finite element models to evaluate structural behavior and experimental setup optimization can complement with the inspector his experience. A new adaptive response surface methodology, especially adapted for thermal problems is used to update the experimental setup parameters in a finite element model to the state of the test sample measured by pulsed thermography. Poly Vinyl Chloride (PVC) test samples are used to examine the results for thermal insulator models. A comparison of the achieved results is made by changing the target values from experimental pulsed thermography data to a fixed validation model. Several optimizers are compared and discussed with the focus on speed and accuracy. A time efficiency increase of over 20 and an accuracy of over 99.5% is achieved by the choice of the correct parameter sets and optimizer. Proper parameter set selection criteria are defined and the influence of the choice of the optimization algorithm and parameter set on the accuracy and convergence time are investigated.

Keywords: finite element method, image processing, infrared thermography, optimization, inverse problem

*Ing. Jeroen Peeters
Email address: jeroen.peeters2@uantwerpen.be (J. Peeters)
URL: www.op3mech.be (J. Peeters)

1. Introduction

The study of Pulsed Infrared Thermography (PT) has become an important Non-destructive Evaluation technique (NDE) for damage detection and material updating in metallic structural components [1, 2, 3], as well as CFRP (Carbon Fiber Reinforced Polymer) and GFRP (Glass Fiber Reinforced Polymer) composites [4]. Thermography has many advantages including non-contact operability, it can be performed in-situ, it can cover large areas and it is a quantitative method [5, 6]. The disadvantages are that defect deeper in the structure are more difficult to inspect [7] and that the results are highly dependent on the used experimental setup conditions, for ex. Emissivity variations and non-homogeneous surface heating. Efficient signal processing and filtering of the defect information in the field of active thermography methods is very important. With the help of adapted image and signal processing algorithms, it is possible to detect small discontinuities inside structures or extract material characteristic information. By reducing the amount of acquired data, the process is accelerated, but a certain decrease in accuracy has to be kept in mind. Quantitative structural health monitoring could be done with the use of high-end post-processing algorithms such as modal analysis, pulsed phase thermography (PPT) and thermal signal reconstruction (TSR) if the material is well known, but the interpretation of the influence of a specific defect on the global behavior of the structure remains difficult and depends on the skills of the inspector. Especially for complex materials such as composite laminates.

Computer simulations are economically interesting and a fast way to determine and simulate material behavior and to calculate worst case scenarios. Finite element (FE) analysis has been used as a verification tool in some applications involving infrared thermography [1, 8, 9, 10]. Besides thermography, FE modeling has proven its success in multiple application areas for worst case simulation and quantitative failure detection. Most of the FE models used in these situations need to be updated to the real conditions of the structure to deliver accurate results. In structural dynamic NDE techniques such as ultrasound vibration C-scanning, this updating process has been well developed and

integrated in FE model updating techniques as described in [11, 12, 13]. As the physics of structural dynamics is described as a second order problem and the thermal behavior of materials as a first order problem, both physics do not follow the same analytic behavior. This is why a different approach to implement FE model updating in thermal problems with a reduced amount of data is needed. Besides that, the parameter selection is not as straight forward as could be expected because of dependencies between the material properties and the surface parameters like the emissivity or heating pattern. For example, thermal conductivity, specific heat capacity and density are interconnected by the thermal diffusivity defined by $\alpha = \frac{k}{\rho C_p}$, but are also influenced by the excitation power as could be seen in Eq.(1). These parameters are fixed for the inspected material but in industrial cases the exact value for each parameter of the inspected structure is unknown and dependent on the material quality. In general the values of the parameters used for FE modeling are selected from datasheets as in [14] which are averaged values from reality. For the accurate use of the FE models, a correct estimation of these material parameters is needed. Further on a variation on the local material thickness of thin structures influences the results of the parameter estimation [15].

In this paper a method is presented to develop an accurate FE model by optimization using reduced PT thermal data for materials with a low thermal conductivity. The method uses a new adaptive response surface optimization algorithm specifically suited for thermal non-linear problems. When using the proposed algorithm, the training time of the inspection is much lower than the method described in [16] by Darabi. The number of function evaluations is significantly reduced by using the response surface as input for the optimization algorithm instead of the complex FE model [17]. FE model updating is well known in ultrasound NDE techniques, where mode shapes and resonance frequencies are used as target data for the optimization strategy [17]. In thermographic measurements this data is not available for updating, as thermal information forms a partial differential first order problem instead of a second order modal problem. The goal of this paper is to find an efficient parameter set and optimizer to use with the specially

designed algorithm to identify changes in the structure, for example delaminations or cracks.

The paper starts with a motivation for the research, followed by a description of the used experimental measurement strategy and the definition of the COMSOL Multiphysics FE model. Next we describe the developed optimization method based on an adaptive response surface method [18, 9]. This method is further developed and redesigned to deliver a robust, global optimization method which uses multiple initial values.

Several issues motivate the present research:

- Extensive calculation time remaining an issue for complex design models in thermography FE simulations. Despite the fast evolution of increasing performance of PCs during the past years, complex FE models with a high number of nodes and elements still suffer from high calculation times in order to solve and combine the necessary internal equilibrium equations [18].

- The accuracy of FE models to estimate realistic behavior of a specific structure is difficult when the material properties of standard material libraries are used. Especially for complex anisotropic materials such as CFRP. When the actual material parameter values for the specific structure are implemented the accuracy of the FE model increases drastically. More and more design departments use FE modeling to improve their products. The models can be reused in further development or maintenance and monitoring steps or for extreme condition simulations on high cost structures but they do not represent the realistic state of the actual produced structure. To correct this inaccuracy between realistic product and design model, the material parameters need to be updated.

- In practical cases a lot of thermographic measurements are performed on complex shaped structures with the same heat source, pulse time and a fluctuating excitation distance which are far from ideal adapted test facilities.

- As quoted from V. Vavilov [19] "The use of the non-linear time domain data for non-linear fitting is the real inversion procedure which delivers the most accurate results but needs a lot of processing time."

2. Test-case description

We used experimental measurement data obtained on a PVC test sample as a low thermal conductive isotropic alternative for carbon laminate structures (CFRP). The benefits of the choice for PVC are the homogenic and isotropic material properties. For verification of the used parameter set a 2D FE model is developed for updating the FE model setup to the actual experimental measurement setup.

2.1. Experimental Setup

In the following subsection it is explained how the experimental measurements are performed in laboratory conditions and the used measurement technique will be described. The experiments are based on active pulsed infrared thermography (PT).

2.1.1. Test sample choice

A flat bottom hole plate, as shown in Fig. 2 was chosen as a test object in the first place to validate the results with the literature [9, 5, 20] and in the second place in order to compare the results with future work. The test sample is made of a low conductive material, PVC to approximate an isotropic 1 dimensional heat flow.

2.1.2. Setup description

Measurements were done in a thermal anechoic chamber with the lights turned off and the operator in a separated room to eliminate reflective hot spots (Fig. 3). The test sample described in section 2.1.1 was placed in a thermal inert frame in the air. Four small nylon connection points were used between the test sample and the supporting frame and the connection points were located below the inspected area of the test sample to avoid thermal influence. The test sample was placed in front of a thermal absorptive wall at a minimum distance of 100 mm. A heating condition with neglectable reflections was

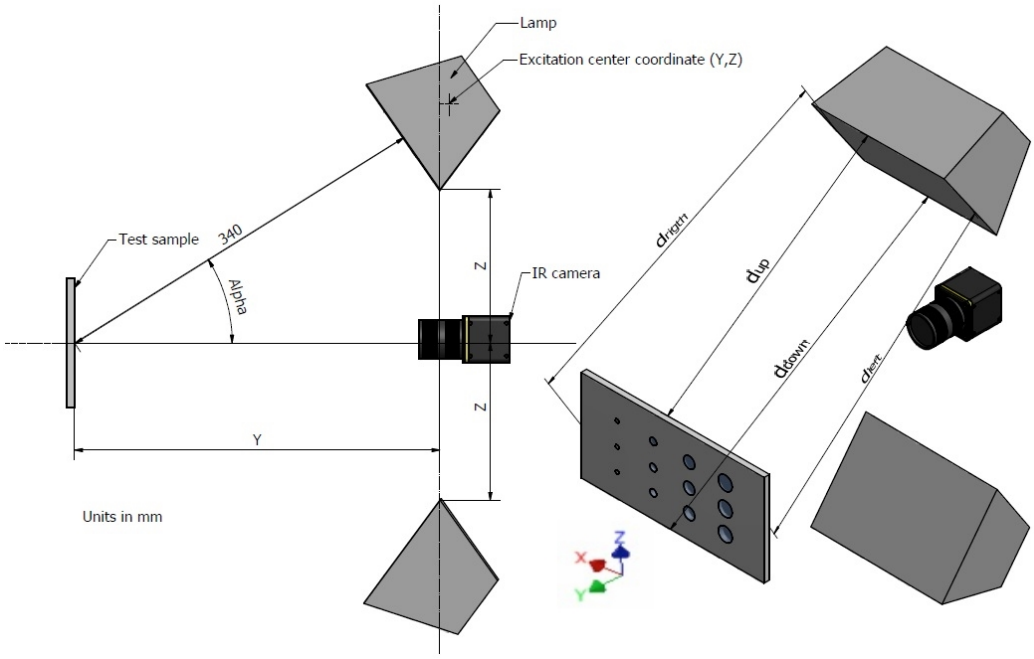

Figure 1: Drawing of the measurement setup, distances in mm. The setup consists of a test sample, two halogen lamps and an IR-camera. Parameters Y, Z and α belong to the parameters as explained in paragraph 2.1.2

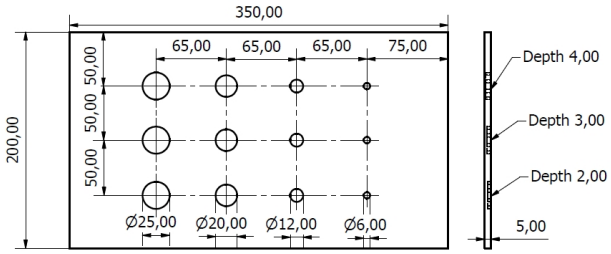

Figure 2: Technical drawing of the Flat Bottom Hole plate.

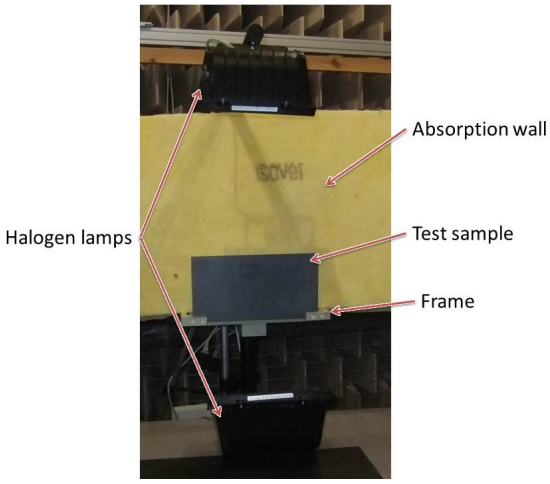

Figure 3: Experimental setup in an anechoic chamber.

realized by orientating the camera and two 1000 W halogen spots under angle α and the camera in front of the test sample as shown in Fig. 1 as explained in [9]. Angle α is, as shown in Fig. 1, the angle between the direct lamp excitation direction and the camera view direction. This results in reflections of the excited heat sources which are not located in the field of view of the camera. Further on the emissivity of the surface should be discussed. As explained in [21], the emissivity should be seen as a local parameter which is spectral-directional dependent. In this study we approximate the inspected material as an optically homogeneous material with smooth surfaces which defines that the emissivity could be defined constant for small normal inspection angles [21]. As explained above, the camera is positioned in front of the test plate. We used a FLIR sc7500 cooled camera with an InSb detector which has a Noise Equivalent Temperature Difference (NETD) of less than 20mK and a frame resolution of 320x256 pixels [22].

2.1.3. Pulsed thermography technique

The used thermographic measuring method is based on pulsed infrared thermography (PT) with a heat pulse length of 5 seconds. An automatic external triggering for correct timekeeping was used and the frame grabbing was synchronized on the same external clock as the excitation trigger. Image capturing was started 20 frames before the excitation source flashes. Image integration was done simultaneously with the image read out of the camera (IWR), so the time inaccuracy of each received frame has to be considered in the FE updating process. How accurate the pulse time could be read out of the thermography measurements is an uncertainty which should be implemented in the FE model. To define the start time of the pulse of the excitation source a mathematical postprocessing of the experimental data was done which uses the first and second derivation of the time signal to measure the trigger time.

The PVC test plates are excited with an excitation time of 5 sec and a total measurement time of 3 minutes and 5 sec. The used frame rate is 10 Hz which results in a total frame amount of 1870 frames. As the lateral heat dissipation could be neglected by the low thermal conductivity, the measurement time should be sufficient to build a proper thermal

profile.

2.2. Finite element model

The Finite Element (FE) models were made using Comsol Multiphysics. This software was chosen because of its integrated connection with Matlab for implementation of the optimization algorithm and because of its equation based approach. In the following subsections we explain how the FE model is designed.

2.2.1. Governing physics

The governing differential equation is a combined heat transfer equation with conduction, convective cooling and radiation of an external heat source, formulated in Eq.(1) and Eq.(2) where ρ is the density, C_p is the heat capacity at constant pressure, T is the absolute surface temperature, κ is the thermal conductivity, t is the time, $Q(t)$ is the time dependent heat source and h is the heat transfer coefficient [23, 24]. The air between the heat sources and the surface is neglected. The simulation set-up is shown in Fig 1. The numerical solution can be considered sufficiently accurate for FE model updating of thermographic NDE applications as described in [16].

$$\rho C_p \frac{\partial T}{\partial t} + \nabla . \left(-\kappa \nabla T\right) = Q \; with \; T\left(x, y, z, 0\right) = T_\infty = 292.88[K] \tag{1}$$

$$\vec{n}(k\nabla T) = h(T_\infty - T) \tag{2}$$

The external heat source has a non-linear characteristic as defined in Eq. (3) where ϵ is the emissivity, F_∞ is the field of view factor of the ambient reflections, σ is the Boltzmann constant, δ is the 3 dimensional power density distribution factor as presented in [25] and P is the power of the heat source [23]. A few simplifications are made:

- The air velocity is assumed to be zero allowed by the laboratory conditions.
- The thermal conductivity κ of PVC is isotropic [26].

- The test sample is opaque and behaves like an ideal grey body as a result of a black paint coating.

$$Q(t) = \epsilon \left(P(t) + F_{\infty}\sigma T_{\infty}^{4} - \sigma T^{4} \right) \; with \; \left\{ \begin{array}{cc} P(t) = \delta * P & for \; t \leq t_{pulse} \\ P(t) = 0 & for \; t > t_{pulse} \end{array} \right\} \tag{3}$$

2.2.2. Model characterization

The FE model consists of 2940 triangular elements with a maximal growth rate of 1.3. The physics is defined by 2 external uniform radiating heat sources defined as described in [9]. The orientation of the heat sources is calculated from the 4 facial distances between the lamp and the test plate as shown in Fig. 1. The coordinates of the source center could be calculated from the set of equations, described in Eq. (4) with as boundary conditions that the sources are placed at the same distance from the sample and pointing towards the center of the sample, which is the origin of our coordinate system in Fig. 1. This results in a set of 3 unknown parameters : Y, Z and the angle α around the x-axis as shown in Fig. 1 and Eq.(4) with L the coordinates of the specific points on the lamp, P the coordinates on the test plate and $d_{rigth},\ d_{left}\ and\ d_{down}$ the distances in meter measured in the test setup as presented in Fig. 1, h the height of the lamp and A the area of the lamp surface. These unknown parameters result in a first parameter set which could be either optimized or kept to a fixed value. These fixed values are determined from the experimental data in a first stage of the described method. Optimization input or measured data are the 3 parameters $d_{rigth},\ d_{left}\ and\ d_{down}\ or\ d_{up}$ as shown in Fig. 1.

In the simulation it is assumed that the heat distribution is uniform and that the heat source housing is an ideal reflector. The temperature data points used for the optimization are placed on a grid with the same spacing as the experimental sensor grid.

The results of the FE model could be evaluated with the use of the real experimental information. This delivers a time efficient and relatively accurate starting FE model. The radiation in the participating media is neglected considering the use of a climatic stable room and sufficiently high excitation power. In reality there is some heat absorption of

the heat source housing and the window in front of the lamp. The stable atmospheric conditions, the distance between the heat sources and the test plate, the short pulse time and the isolation of the stationary air make this effect neglectable. The heat source body also has radiative and convection losses. These are limited by the short pulse time and the thermal resistance of the window in combination with the thermal stable room parameters. Besides that the halogen sources are not thermally isolated from the environment. Thereby there is a heat flux from the sources to the ambient which cools down the heat sources. Between two experiments all environmental parameters were stabilized to perform accurate measurements. Thereby the radiative and convective losses of the heat sources to the environment are neglected in the experiments.

$$\left\{\begin{array}{c} d_{rigth} = 0.35 = \sqrt{(L_{right,(y,z)} - P_{right,(y,z)})^2} \\ d_{left} = 0.35 = \sqrt{(L_{left,(y,z)} - P_{left,(y,z)})^2} \\ d_{down} = 0.30 = \sqrt{(L_{down,(y,z)} - P_{down,(y,z)})^2} \\ L_{up,y} = L_{left,y} - h/2 * sin(\alpha) \\ L_{down,y} = L_{left,y} + h/2 * sin(\alpha) \\ L_{rigth,(y,z)} = L_{left,(y,z)} \\ L_{down,z} = L_{left,z} + h/2 * cos(\alpha) \\ L_{up,z} = L_{left,z} - h/2 * cos(\alpha) \\ Y = \frac{1}{A} \int_L y \, dA \\ Z = \frac{1}{A} \int_L z \, dA \end{array}\right\} \tag{4}$$

3. Methodology

Both the quality of the experimental data and the FE model data will contribute to the evolution of the optimization algorithm. The implemented optimization algorithm is based on the adaptive response surface method described in [17, 18, 9]. We made some modifications and extensions to the algorithm which are especially designed for thermographic applications.

3.1. Adaptive response surface method

For the optimization algorithm noise filtered experimental data is used as target for the FE model. The optimization uses the relative temperature differences $\theta = T - T_0$ to reduce the measurement uncertainties. A full overview of the method is described in the flowchart in Fig. 4. The algorithm has no fixed amount of iterations in contrast to the method described in [18]. As could be seen on Fig. 4, if the tolerated accuracy is smaller than the error of the optimization, than the algorithm needs to proceed its iterations, unless the improvement between consecutive iterations is to small. If the error of the optimization algorithm is smaller than the tolerated accuracy or the improvement between two consecutive iterations is too small, the iteration process is completed. The parameter stability control is increased in contrast to the method described in [9] by the choice of independent parameter sets and the use of multiple initial value for each parameter set.

As could be seen in Fig. 4, in a first stage a meta model is created of a response surface built from $2 * n - 2$ data points for $n > 2$, retrieved from random distributed FE simulations across the design space. The design space is built from the physical boundary values for each parameter of the objective function. This meta model consists of n-dimensional polynomials, each dimension represents an unknown parameter and in total they form one single n-dimensional response surface. The optimization algorithm searches for a global minimum of the objective function in the meta model which results in estimated values for each parameter. The retrieved estimated parameter values of the minimum are the input of a new FE model, called the updated FE model as could be seen in Fig. 4. The results of this updated FE simulation have a higher correlation with the experimental target values and deliver new input for the meta model which could replace the least accurate data point inside the meta model with the higher accurate data point of the last simulation. This delivers a new point in the meta model which reforms the response surface locally in the region of the extra data point. Thereby a so called pan & zoom effect occurs where only the most relevant data points are considered to build the meta model and an increased accuracy is achieved. The local conversion of the response surface is a local solution of the optimization problem. The use of different initial values at the same time delivers

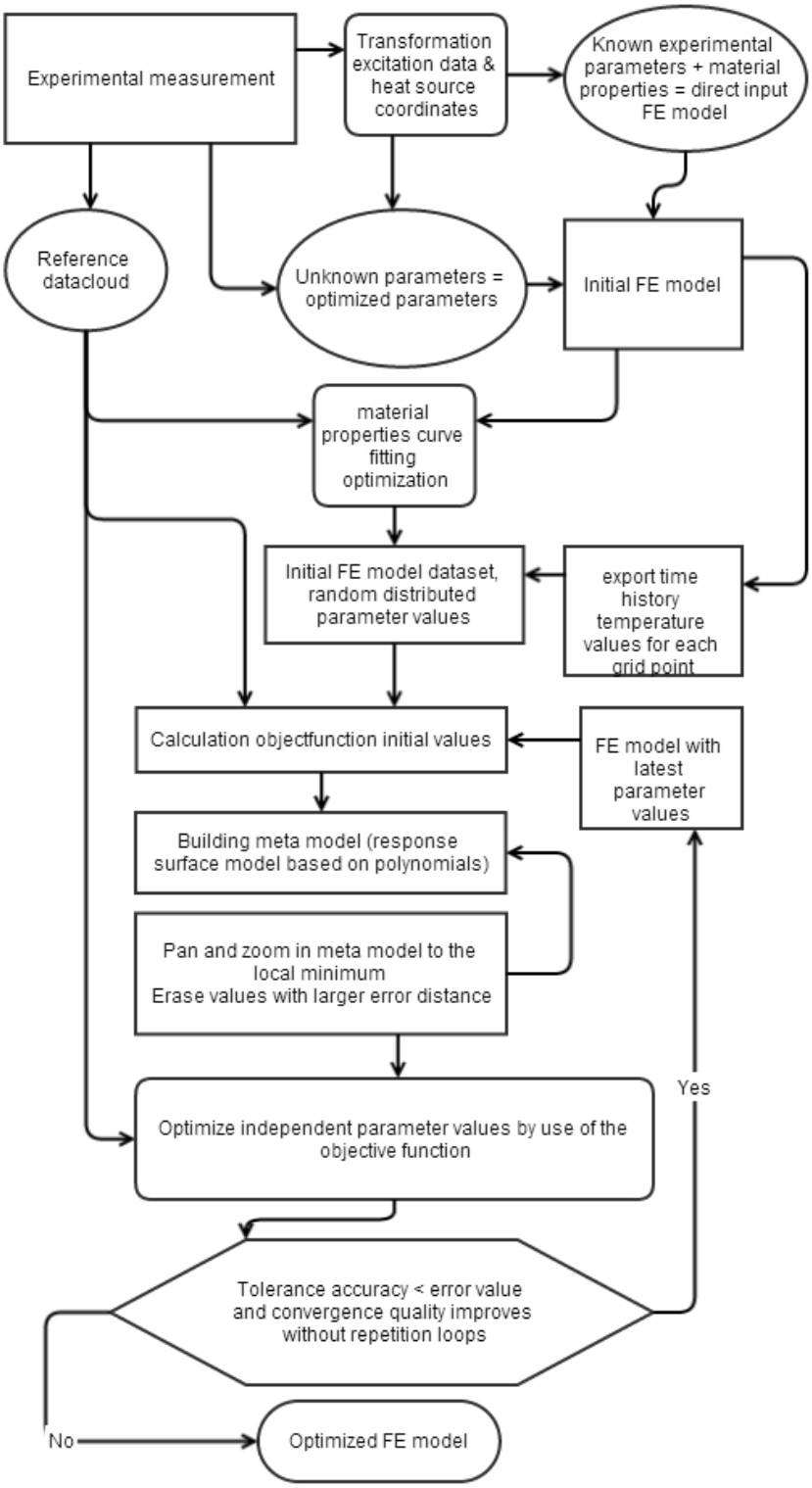

Figure 4: Schematic overview of the optimization method.

a conversion to a global optimum. This process continues until convergence is achieved for the error value between the experimental value and the minimum of the meta model. In this study the threshold value for convergence is placed on $5e^{-3}$ maximum error value for 90 time steps on the normalized parameters following Eq(5). The threshold value is based on the accuracy of the FE model fixed in the FE simulation software and based on a convergence study for the used mesh. This convergence study resulted in an approximated minimal error of $5e^{-3}$.

$$Error = \sum_{t=0}^{frames} T_{comsol}(t) - T_{exp}(t) \tag{5}$$

3.1.1. Optimized parameters choice

The choice of a suitable parameter set is one of the most critical steps in the optimization routine. In a first step the parameters as defined in Table 1 and Table 2 were used as one parameter set in the main optimization step. As presented in Fig.5 the parameters of Table 1 result in an unstable optimization routine whereby the spatial temperature data in function of the time is insufficient to solve the optimization problem. As shown in Fig. 5 there are more mathematically correct answers, plotted in white, to this problem with only one physically correct answer. This is a result of the dependency between the parameters. For present work the exact value of each material property is not essential. Each value of the described parameter set of Table 1 which is a solution of Eq.(6) is a possible result.

$$T_{exp}(t) = T_{FE}(t, k, C_p, \varepsilon, \rho, P) \tag{6}$$

The optimization strategy is divided in three stages, described in the flowchart of Fig. 4 as the rounded rectangles.

1. The pulse start time is a result of the second derivative calculation of the experimental data as shown in Fig. 6, which forms the input of the global optimization routine. As could be seen, the start pulse is calculated after $2sec$, on 10Hz this results in 20 frames as start frame of the excitation pulse as explained in section 2.1.3. The

lamp coordinates are calculated following the described equation set Eq.(4) with as unknown parameter the length of Y which is measured as $Y = 0.3496m$.

2. The parameter set of Table 1 is optimized to a solution following Eq.(6) which delivers a correct curve fitting between the experimental data and the FE model for each value of the parameters of Table 2. The lower and upper boundaries of the different parameters are based on extrema mentioned in data sheets and references cited in [14, 21].
3. The exact values of the independent parameter set of Table 2 are calculated using the optimization algorithm.

We thereby receive a 1D heat transfer with a 3D global optimization problem whereby independent parameters as the source coordinates and the pulse start time are calculated separately out of the experimental measurement data.

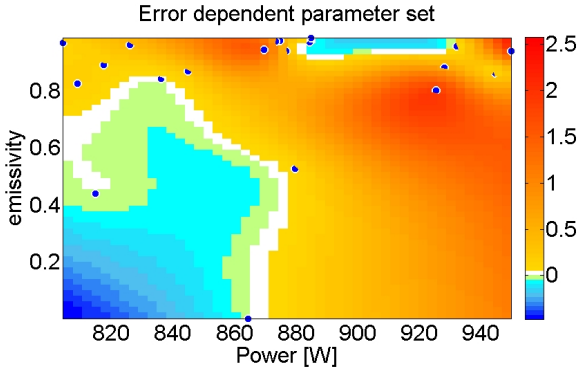

Figure 5: Error plot of the parameters of Table 1. All solutions with equal results are indicated in white.

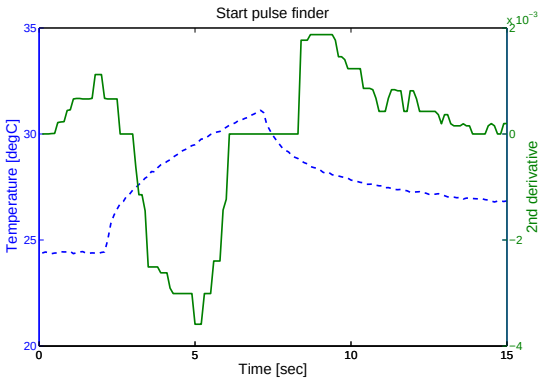

Figure 6: In the experiment, the start of the pulse time is determined after the first top of the second derivative (solid) of the temperature-time signal(–).

3.1.2. Objective function

The used objective function consists of:

- The minimization function to locate the minimum of the response surface as defined in Eq.(7) where $\ell(\vartheta)$ is defined as the objective function which should be minimized.

Table 1: Dependent optimization parameters with their boundary conditions for PVC [14].

Parameter	Lower boundary	upper boundary
Heat source power $[W]$	900	1000
Thermal conductivity PVC $k[W/(m.K)]$	0.12	0.209
Specific heat capacity PVC $C_p[J/(Kg.K)]$	1000	1800
Density PVC $\rho[kg/m^3]$	1290	1560
Heat transfer coefficient $W/(m^2.K)$	5	30
Emissivity	0.80	0.95

Table 2: Independent Optimization parameters with their boundary conditions for PVC.

Parameter	Lower boundary	upper boundary
Ambient Temperature $T_\infty[K]$	273.15	300.15
Hole thickness $d[mm]$	0.10	4.80
Pulse Time PVC $t_{pulse}[s]$	3.5	6.5

T is the relative temperature, respectively for the experimental target data set and the approximated model, where the relative temperature results of the model are dependent on the optimized parameters ϑ.

- An equation which defines the inequality of the hole depth related with the total plate thickness.
- The solution of Eq.(4) to define the coordinates and orientation of the heat sources.

Next the objective function is used to test if the boundary conditions are not violated. If so, the closed boundary is calculated and the parameter value is set to the boundary value including an internal weighting factor which makes the specific parameter and its boundary conditions more important.

$$\ell(\vartheta) = T_{model}(\vartheta) - T_{Ex} \tag{7}$$

3.1.3. Optimizers

Three gradient based optimizers are compared and investigated to find which one of them delivers the fastest and most accurate results. The optimization strategies are all designed for non-linear, continuous problems with a continuous first derivative and are chosen for their stability and robust object function adaptation. As first optimizer use is made of a non-linear minimal constraint optimizer for multivariate problems, implemented as shown in Eq.(8) with *ceq* defined as the equation set described in Eq.(4), $c(\vartheta)$ a test function in function of the optimized parameters ϑ and lb and ub the physical limits of the parameters as defined in Table 2. In the optimizer use is made of the interior-point algorithm to handle the problem and to restore the optimization if the FE software delivers semi-infinite values. Further on the algorithm is adapted for large scale problems which is the case for long measurements. [27, 28, 29]

$$\min_{\vartheta} \sum_{i=0}^{t} \ell_i(\vartheta) \; with \begin{cases} c(\vartheta) \leqslant 0 \\ ceq(\vartheta) = 0 \\ lb \leqslant \vartheta \leqslant ub \end{cases} \tag{8}$$

The second optimizer uses a nonlinear least-squares strategy for data-fitting as defined in Eq.(9). Within this optimizer there is made use of the Trust-region reflective and the Levenberg-Marquardt algorithms, both based on the Gauss-Newton method. Thereby the Trust-region reflective is especially adapted for the use of bound constraints and the Levenberg-Marquardt algorithm for under-determined problems. More information about the algorithms can be found in [27, 28, 30, 31].

$$\min_{\vartheta} \; \|(\ell_i(\vartheta)\|_2^2 \; with \; lb \leqslant \vartheta \leqslant ub \tag{9}$$

The last chosen optimizer is an adaptation of the non-linear least-squares strategy especially designed for curve fitting problems, defined in Eq.(10) whereby the objective function delivers predictions of the temperature values instead of the error function as described in Eq.(7). The main difference between this optimizer and the previous one is the absences of weighting factors. The use of time dependent curve fitting should results in

more stable and robust results as mentioned in bullet 4 in section 1 referred to V. Vavilov [19]. Both algorithms as described above are used with this optimizer. [27]

$$\min_{\vartheta} \sum_{i=0}^{t} (T_{FE,i}(\vartheta, t) - T_{Ex,i})^2 \; with \; lb \leqslant \vartheta \leqslant ub \tag{10}$$

4. Results and discussion

In this section there is first made a comparison between two 2D FE models of the flat bottom hole plates as described in 2.2. The first, fixed FE model has an arbitrary set of values for the defined optimization parameters ϑ. The second, updated FE model will start from a randomly chosen start position to update to the same values of the parameters of the fixed FE model. With these measurements the convergence between different start values and optimization strategies is validated. The results are shown in Table 4 with the FMC (minimal constraint) optimizer, the Lsq (Least-square) optimizer and the LCF (Least-square curve fitting) optimizer and the LM (Levenberg-Marquardt)algorithm and the TRR (Trust-region reflective) algorithm. The column FE-LCF TRR is an optimization routine whereby the meta-model building is bypassed and every iteration calculates a FE model. We know that each FE simulation consumes $5.65 seconds$ calculation time and that the simulation duration for each FE model call is the same, independent of the parameter values. As could be seen in Table 3 the amount of called FE solves with and without the use of the algorithm delivers a large efficiency increase. A same time efficiency increase could be seen in [18]. Further on we can see that the relative time consumption of the FE simulations decreases less than the time efficiency increase of approximately a factor 20.

As shown in Table 4, all optimization methods deliver good convergence with less than 1000 iterations to an accuracy smaller than 0.005 as mentioned in section 3.1. The residuals are calculated as a summation of the residual of the objective function for each time step. The validation measurements are done for 90 time steps which results in a summarized difference over the full time loop. However the necessary amount of iterations differs a lot with the choice of optimizer chosen in the global optimization loop. By the discussion of

Table 3: Simulation duration comparison

	Full optimization	with use of response surfaces
Iterations	54	47
amount of FE calls	1039	47
Average amount of simulations in each iteration	19.2	1
Total duration	10 432.8	522.35
Percentage of time used for simulations	56.3%	50.8%

Table 4: Results validation optimization method between 2 FE models.

Optimization method	Target	FE-LCF TRR	FMC	Lsq TRR	Lsq LM	LCF TRR	LCF LM
Temperature $T_\infty[K]$	293.15	293.17	293.16	293.15	293.15	293.15	293.15
Hole thickness $d[mm]$	1.00	0.9980	1.0020	0.99562	1.0346	1.0105	0.99257
Pulse Time $t_{pulse}[s]$	2.50	2.5802	2.4996	2.5094	2.4916	2.4935	2.5005
Iterations	/	54	960	994	360	47	195
Residuals	/	4.9906e-3	4.9548e-3	4.9975e-3	4.9996e-3	4.9616e-3	4.9815e-3
Time $[s]$	/	10 432.8	10 603	9 685.3	3 534.4	522.35	1 949.1

these results we have to keep in mind the few assumptions made in section 2.2 and the 1 dimensional character of this problem. The lateral diffusion is assumed to be zero. This assumption is allowed by the use of a high thermal insulator material. These results proof that the updating strategy works for measurements with a low noise level, providing the first necessary verification. A graphical presentation of the convergence of all strategies is presented on a double logarithmic scale in Fig. 7. By comparison of the normal least squares strategy (Lsq) with the adapted curve fitting optimizer (LCF) it could be seen that the amount of necessary iterations is until 20 times smaller and the calculation time of one iteration is for all the same which results in an overall solution time decrease. Further it could be seen in Fig. 7 that the LM algorithm is a little slower in the beginning and at the end than the TRR algorithm. This is expected and is known for the reason that the TRR method increases its step size in the beginning when the initial values are far away of the optimum [32]. The minimal constraint optimizer (FMC) needs the most iterations to

achieve the expected accuracy. We can conclude that the expected convergence as described in 3.1 is achieved for noise free data.

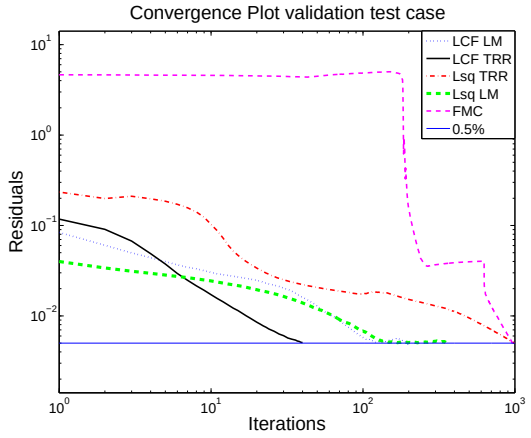

Figure 7: Convergence graph of the validation test case.

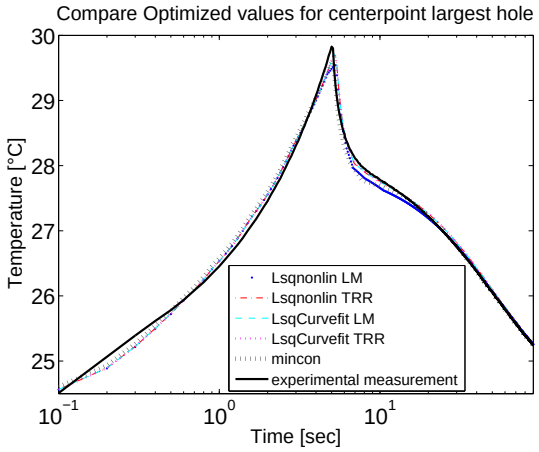

Figure 8: Time plot of the temperature profile in function of the time for center of the largest flat bottom hole in the experimental test case.

As second stage the same optimization strategies are used with raw experimental data as described in the section 2.1 with the optimized FE model. This includes noise in the target data and thereby the stablity of the update algorithm is tested. This is done for a test sample as described in section 2.1.1. As expected there are more iterations needed to let the solution converge by the influence of the noise. The results are presented in Table 5. As could be seen, the used tolerance is changed from 0.005 to 0.05 for the reason that the residual values of the validation test case are calculated as a summation of 90 time steps and the residual value of the PVC test case are a summation of 900 time steps, which results in a comparable accuracy. A representation of the time plots for the largest and deepest hole is given in Fig. 8. This figure shows the fitting of all optimizers is sufficient but the LCF TRR delivers the best fit. Besides the accuracy is not only dependent on the optimization method but also on the amount of noise in the experimental data, a similar accuracy is achieved. There could be seen that with the implementation of the noise the amount of necessary iterations is far closer than in the previous test case. A possible explanation

Table 5: Results experimental optimization method for PVC sample.

Optimization method	Target	FMC	Lsq TRR	Lsq LM	LCF TRR	LCF LM
Temperature $T_\infty[K]$	297.66 ± 0.02	297.68	297.67	297.67	297.67	297.67
Hole thickness $d[mm]$	0.99 ± 0.01	0.95	0.99	0.99	0.99	0.99
Pulse Time $t_{pulse}[s]$	5.5 ± 0.5	5.2	5.3	5.3	5.3	5.3
Iterations	/	1276	1045	1068	857	1034
Residuals	/	1.9458e1	4.9996e-2	5.0000e-2	4.9999e-2	4.9993e-2
Time $[s]$	/	11 670	9 441.4	9 819.6	7 671.1	8 860.5

therefore could be that the Lsq optimizer is more appropriate for noisy data then the LCF optimizer. The FMC data delivers the worst results, with a residual value that is almost 40 times higher. A possible reason is that the summation before the optimization delivers a decrease in sensitivity for the time data and an increased sensitivity for the small overall differences as result of the noise. This in combination with the noise could explain the bad accuracy. This results deliver interesting results to use for FE updating of thermal insulator materials for global parameters with a 1 dimensional thermography measurements. It is proven that the use of noisy experimental data is possible to estimate the optimized parameters. A representation of the response surface for the 3 optimized parameters with the LCF TRR optimizer is shown in Fig. 9. In Fig 9a is seen the piece of the response surface for the ambient temperature and the thickness parameter, in Fig. 9b the response surface is plotted for the ambient temperature and the pulse time parameter.

5. Conclusions

This paper presents the use of a new adaptive response surface method for thermal optimization of geometrical parameters to the experimental values, measured by pulsed thermography on materials with low thermal conductivity. The method is based on a division of the unknown parameters into two different categories, one parameter set of which the exact value is important for the FE updating of the geometry and experimental case and one parameter set of which the values are out of the scope of the investigation but

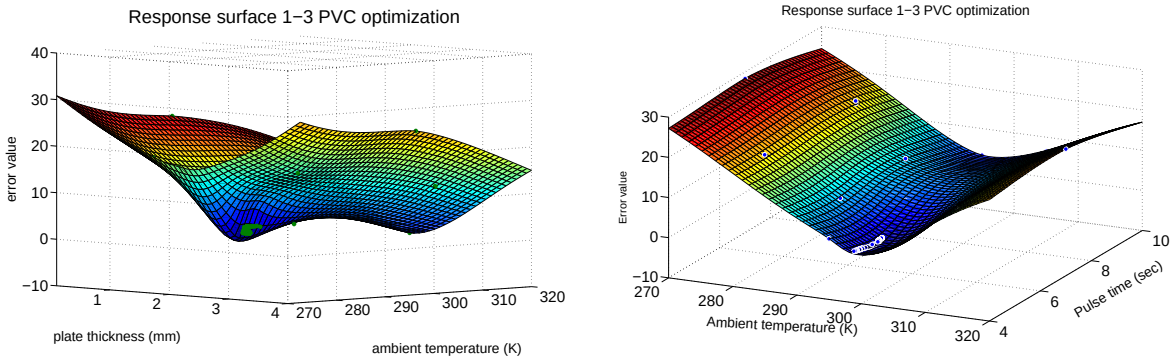

(a) The response surface of the ambient temperature versus the material thickness.

(b) The response surface of the ambient temperature versus the pulse time.

Figure 9: The response surface of the error value at the puls time for all parameters of the PVC test case, plotted for the LCF TRR optimizer.

which influences the accuracy of the results. From the results we can conclude that the use of the optimization algorithm speeds up the convergence and results in a time reduction of factor 20 with respect to an optimization without the use of a response surface. The dependency of the used optimization algorithm and optimizer were investigated. The use of a least square curve fitting optimizer with a trust region algorithm was found to be the most appropriate for thermography test cases. In addition there is no loss in accuracy for noise free data. With the implementation of noise the accuracy decreases but the parameter estimation keeps sufficient for FE updating. The test case on a simplistic material with low thermal conductivity demonstrates the usefulness for computation-intensive design problems with thickness and material differences on homogeneous thermal insulator materials in laboratory conditions. When extrapolating the results to materials with high thermal conductivity, larger differences between the experimental and simulation results can be expected. In that case the assumption of no lateral heat dissipation cannot be made. Also the definition of the time stepping in the FE model is more crucial than with insulator materials. Further research is necessary to estimate if the same algorithm can be used or that some improvements are needed to implement the lateral diffusion in the problem. For low conductive materials where this assumption is valid, the optimization algorithm

can deliver good approximations of unknown ambient parameters and material thicknesses. Also for an-isotropic materials like CFRP, the method has its benefits to estimate layup properties and laminate properties. The optimized model could be used in failure detection or other IR based image analysis to assist the IR measurements and combine the benefits of surrogate modeling (fast and economical efficient) with IR NDE for quantitative detection of the influence of changed material conditions and FE model updating. It is also made possible to adapt the setup conditions of the FE model to the realistic state of the test sample or to define the most efficient measurement setup for a specific structure. This concludes that the described method could be used to improve the experimental test setup with the use of an accurate FE model to improve the non-destructive testing of complex shaped structures.

Acknowledgements

This research has been funded by the University of Antwerp and the Institute for the Promotion of Innovation by Science and Technology in Flanders (IWT) by the support to the TETRA project 'Smart data clouds' with project number 140336. Furthermore, the research leading to these results has received funding from Industrial Research Fund FWO Krediet aan navorsers 1.5.240.13N. The authors also acknowledge the Flemish government (GOA-Optimech) and the research councils of the Vrije Universiteit Brussel (OZR) and University of Antwerp (fti-OZC) for their funding.

Bibliography

[1] P. Chaudhuri, P. Santra, S. Yoele, A. Prakash, D. C. Reddy, L. Lachhvani, J. Govindarajan, Y. Saxena, Non-destructive evaluation of brazed joints between cooling tube and heat sink by ir thermography and its verification using fe analysis, NDT & E International 39 (2) (2006) 88–95.

[2] M. Vollmer, K.-P. Möllmann, Infrared thermal imaging: fundamentals, research and applications, John Wiley & Sons, 2010.

[3] W. Jeong, C. Earls, W. Philpot, A. Zehnder, Inverse thermographic characterization of optically unresolvable through cracks in thin metal plates, Mechanical Systems and Signal Processing 27 (2012) 634–650.

[4] M. Susa, C. Ibarra-Castanedo, X. Maldague, S. Svaic, I. Boras, A. Bendada, Pulse thermography applied on a complex structure sample: comparison and analysis of numerical and experimental results, in: IV Pan American Conference in END, Buenos Aires, Argentina, 2007.

[5] C. Ibarra-Castanedo, M. Genest, J.-M. Piau, S. Guibert, A. Bendada, X. P. Maldague, C. Chen, Active infrared thermography techniques for the non-destructive testing of materials, Capter XIV of the book:Ultrasonic and Advanced Methods for Nondestructive Testing and Material Characterization, ed. Chen CH (2007) 325–348.

[6] G. Giorleo, C. Meola, Comparison between pulsed and modulated thermography in glass–epoxy laminates, NDT & E International 35 (5) (2002) 287–292.

[7] G. Busse, Techniques of Infrared Thermography: Part 4. Lock-in thermography, in: Nondestruct. Handb., 3rd Edition, ASNT Press, Columbus, Ohio, 2001, p. 718.

[8] M. Louaayou, N. Naït-Saïd, F. Z. Louai, 2d finite element method study of the stimulation induction heating in synchronic thermography ndt, NDT & E International 41 (8) (2008) 577–581.

[9] J. Peeters, G. Steenackers, B. Ribbens, G. Arroud, J. Dirckx, Finite element optimization by pulsed thermography with adaptive response surfaces., in: QIRT 2014, paper 039, Bordeaux (France), 2014, p. 10.
URL http://qirt.org/archives/qirt2014/QIRT 2014 Papers/QIRT-2014-039.pdf

[10] C. Earls, Stochastic inverse thermographic characterization of sub-pixel sized through cracks, Mechanical Systems and Signal Processing 30 (2012) 146–156.

[11] M. Friswell, J. E. Mottershead, Finite element model updating in structural dynamics, Vol. 38, Springer, 1995.

[12] T. Marwala, Finite Element Model Updating Using Computational Intelligence Techniques: Applications to Structural Dynamics, Springer, 2010.

[13] R. Sun, G. Chen, H. He, B. Zhang, The impact force identification of composite stiffened panels under material uncertainty, Finite Elements in Analysis and Design 81 (0) (2014) 38 – 47.

[14] Granta, PVC (chlorinated , molding and extrusion) (2013).

[15] I. Martinez, Heat transfer and thermal radiation modelling (2014).

[16] A. Darabi, X. Maldague, Neural network based defect detection and depth estimation in tnde, NDT & E International 35 (3) (2002) 165–175.

[17] G. Steenackers, R. Versluys, M. Runacres, P. Guillaume, Reliability-based design optimization of computation-intensive models making use of response surface models, Quality and Reliability Engineering International 27 (4) (2011) 555–568.

[18] G. Steenackers, F. Presezniak, P. Guillaume, Development of an adaptive response surface method for optimization of computation-intensive models, Computers & Industrial Engineering 57 (3) (2009) 847–855.

[19] V. Vavilov, W. Ś, D. Derusova, Ultrasonic and optical stimulation in IR thermographic NDT of impact damage in carbon composites, in: QIRT 2014, paper 58, Bordeaux, 2014, pp. 2–6.

[20] X. Maldague, F. Galmiche, A. Ziadi, Advances in pulsed phase thermography, Infrared physics & technology 43 (3) (2002) 175–181.

[21] X. Maldague, Theory and practice of infrared thermography for nondestructive testing, Wiley, Quebec, 2001.

[22] FLIR, The Ultimate Infrared Handbook for R & D Professionals (2010).

[23] A. J. Chapman, Heat transfer, 4th Edition, Macmillan, New York, 1984.

[24] B. Stotter, K. Gresslehner, G. Mayr, G. Hendorfer, J. Sekelja, Quantitative application of pulse phase thermography to determine material parameters, in: QIRT 2014, paper 74, Bordeaux (France), 2014, p. 10.
URL http://qirt.org/archives/qirt2014/QIRT 2014 Papers/QIRT-2014-074.pdf

[25] B. Wang, Chip-Level Thermal Analysis, Modeling, and Optimization Using Multilayer Green's Function, 2008.

[26] P. Dashora, G. Gupta, J. Dashora, Thermal conductivity, diffusivity and heat capacity of plasticized polyvinyl chloride, Indian Journal of Pure and Applied Physics 43 (2) (2005) 132–136.

[27] The MathWorks, The Matlab user manual (2013).

[28] T. F. Coleman, Y. Li, An interior trust region approach for nonlinear minimization subject to bounds, SIAM Journal on optimization 6 (2) (1996) 418–445.

[29] R. H. Byrd, M. E. Hribar, J. Nocedal, An interior point algorithm for large-scale nonlinear programming, SIAM Journal on Optimization 9 (4) (1999) 877–900.

[30] S. Wright, J. Nocedal, Numerical optimization, Vol. 2, Springer New York, 1999.

[31] D. Marquardt, An algorithm for least-squares estimation of nonlinear parameters, J. Soc. Ind. Appl. ... 151 (3712) (1963) 859–60. doi:10.1126/science.151.3712.859-b.

[32] F. V. Berghen, Levenberg-marquardt algorithms vs trust region algorithms (2004).